

Electromagnetic induction in a generalized 3D anisotropic earth, Part 2: The LIN preconditioner

Chester J. Weiss* and Gregory A. Newman*

ABSTRACT

A practical limitation in the use of generalized 3D forward modeling algorithms for inversion of electromagnetic data is the high computational cost of solving large, ill-conditioned systems of linear equations arising from the discretization of the governing Maxwell equations. To address this problem, a new class of preconditioners has recently been proposed which is based on a Helmholtz decomposition of the electric field in the low induction number (LIN) regime. This paper further develops that idea and introduces a LIN preconditioner which can be applied to problems characterized by a fully generalized anisotropic medium. Included are sample calculations demonstrating a reduction by two orders of magnitude in the number of “quasi-minimal residual” iterates and a speedup by a factor of approximately four in the solution time for one forward calculation. Also included are results previously unobtainable by standard Jacobi preconditioning for simulating multicomponent induction sonde response in a horizontal well within a crossbedded formation.

INTRODUCTION

The presence of electrically anisotropic earth materials can have a profound effect on the interpretation of electromagnetic (EM) data. Examples where this is the case are spread throughout the range of geologic sciences from studies on the evolution of oceanic crust (Everett and Constable, 1999) to the analysis of induction log data (Klein, 1993) to aquifer mapping (Christensen, 2000). Recent advances in modeling low-frequency EM induction in a fully generalized 3D anisotropic medium (Davydycheva and Druskin, 1999; Weidelt, 1999; Wang and Fang, 2001; Weiss and Newman, 2002) have been motivated largely by the desire to minimize uncertainty in the interpretation of EM data where anisotropy effects are believed to be significant. Some progress can be made towards

improved interpretations of EM data through the accumulation of response curves for a given EM instrument and a suite of geologic scenarios. Additional progress may be realized through the application of geophysical inversion techniques. Regardless, building a comprehensive catalog of response curves and the efficient execution of an inversion algorithm both rely on speedy forward calculations. We present here a method for significantly reducing the calculation time of 3D finite-difference (FD) simulations which prove useful in either of these endeavors. Furthermore, we also present a sample calculation of the multicomponent induction coil response within a horizontal well embedded in an anisotropic medium. Studies by Yu et al. (2001) demonstrate that multicomponent induction coils can recover the formation anisotropy parameters of thinly bedded turbidite sequences. The example presented here considers the more complicated case of the crossbedded sandstone unit which draws analogy from the well-known hydrocarbon reservoirs of eolian origin such as the Permian-Pennsylvanian Casper sandstone in southeastern Wyoming (Steidmann, 1974), the Jurassic Nophlet sandstone in southern Mississippi and Alabama (Berg, 1986), and the Permian Rotliegendes sandstone in the North Sea Basin (Glennie, 1972).

To address the problem of slow convergence in the iterative solution to finite difference equations at frequencies less than 1 MHz, Newman and Alumbaugh (2002) introduced a “low induction number” (LIN) preconditioner based on the Helmholtz decomposition of the electric fields in the static limit. When compared to simple Jacobi scaling, the LIN preconditioner resulted in a speedup in the solution time by a factor of 10 for a dipping borehole problem in a transversely anisotropic medium. Their work on preconditioning closely parallels that of Druskin et al. (1999), who used the same decomposition, coupled with the inverse of the discretized curl-curl operator, to construct various Krylov subspaces which resulted in a factor of 100 speedup of the spectral Lanczos decomposition method (Druskin and Knizhnerman, 1988). This improvement to the spectral method does not restrict its ability to remove spurious modes or its property whereby solutions for

Manuscript received by the Editor March 8, 2002; revised manuscript received November 1, 2002.

*Sandia National Laboratories, Geophysical Technology Department, Post Office Box 5800, MS 0750, Albuquerque, New Mexico 87185-0750.
E-mail: cjweiss@sandia.gov.

© 2003 Society of Exploration Geophysicists. All rights reserved.

multiple frequencies can be obtained for a cost that is only slightly greater than that for a single frequency.

While other preconditioners (e.g., polynomial, block Jacobi, and Choleski) have been investigated within the confines of the geophysical EM induction problem (c.f., Mackie et al., 1994; Newman and Alumbaugh, 1996), the reduction in solution time they provide is much less than the factor of 10–100 realized by the Helmholtz decomposition techniques. Improvements in the coverage rate of the bi-conjugate gradient method are reported by Smith (1996) when a static divergence correction is applied intermittently during iterative sequence, resulting in a factor of 2–4 in speedup of the solution time.

This paper extends the treatment of the LIN preconditioner to an anisotropic medium characterized by a dense 3×3 conductivity tensor $\bar{\sigma}$. Particular attention is paid to a finite difference discretization of the $\nabla \cdot \bar{\sigma} \nabla \phi$ term which appears in the LIN preconditioner and also in the auxiliary problem of dc resistivity simulations. We begin with an introduction to the governing partial differential equation (PDE) for low-frequency electromagnetic induction in an anisotropic conducting medium. Brief discussions follow on discretizing the PDE using the staggered FD method and preconditioning the resulting system of linear equations in the context of iterative Krylov method solvers. Next, the FD equations of the LIN preconditioner are derived for a generalized 3D anisotropic medium. Examples are then presented comparing the performance of the LIN preconditioner to Jacobi preconditioning. Last, the response of a crossbedded sandstone unit containing a horizontal well is evaluated, and the 3D effects due to the formation anisotropy are quantified. Comments on these results are contained in the Discussion section; the salient points of the paper and their implications are summarized in the Conclusions section. For convenience, a full derivation of the LIN preconditioner is included in the Appendix.

THEORY

The governing equation for the distribution of electric field \mathbf{E} throughout an anisotropic medium is derived from Maxwell's equations as

$$\nabla \times \nabla \times \mathbf{E} + i\omega\mu\bar{\sigma}\mathbf{E} = -i\omega\mu\mathbf{J}, \quad (1)$$

where an $\exp(i\omega t)$ time dependence is implicit. In the case of a total field formulation, the vector field \mathbf{J} represents the source currents responsible for the generation of eddy currents throughout a medium characterized by a symmetric 3×3 electrical conductivity tensor $\bar{\sigma}$ and constant magnetic permeability μ . For a scattered field formulation, \mathbf{J} is defined as $(\bar{\sigma} - \sigma_0)\mathbf{E}^b$, where \mathbf{E}^b are the known electric fields generated by a reference conductivity model σ_0 which is often simpler than $\bar{\sigma}$, and thereby offers the solution \mathbf{E}^b with comparatively little effort. In this latter case, the total electric field is given by sum $\mathbf{E} + \mathbf{E}^b$.

Discretization of equation (1) by a staggered FD grid (Yee, 1966) with symmetric scaling (Newman and Alumbaugh, 1995; Weiss and Newman, 2002) yields a large-scale ill-conditioned system of linear equations,

$$\mathbf{A}\mathbf{x} = \mathbf{b} \quad (2)$$

where \mathbf{A} is a complex symmetric matrix, \mathbf{x} is the vector of electric field components, and \mathbf{b} is the vector of source components. A computationally efficient algorithm for solving systems of this type is the quasi-minimal residual (QMR) method

(Freund and Nachtigal, 1994), which belongs to the class of iterative Krylov subspace methods that includes conjugate gradient (CG) methods. As is the case with all Krylov methods, the rate at which the approximate solutions \mathbf{x}_i converge toward the actual solution is dependent upon the condition number $\|\mathbf{A}^{-1}\|_p \|\mathbf{A}\|_p$, where $\|\cdot\|_p$ denotes some p -norm. Matrices with small condition numbers tend to converge rapidly, whereas those with large ones (as is the case here) converge slowly, if at all.

One way to improve the slow convergence rate for the system in equation (2) is to transform it by a symmetric matrix, \mathbf{C} into an equivalent system,

$$(\mathbf{A}\mathbf{C}^{-1})(\mathbf{C}\mathbf{x}) = \mathbf{b}, \quad (3)$$

where the condition number of $\mathbf{A}\mathbf{C}^{-1}$ is, hopefully, smaller than that of \mathbf{A} . A useful feature of the QMR algorithm is that we can solve the transformed system [equation (3)] while avoiding computing the computationally expensive matrix-matrix product $\mathbf{A}\mathbf{C}^{-1}$. Instead, the effect of the transformation in equation (3) is realized by computing the action of the preconditioner \mathbf{C}^{-1} at each step i of the iterative sequence on the i th Lanczos vector \mathbf{v}_i [see algorithm 8.1 in Freund and Nachtigal (1994)]. Thus, at each step of the QMR sequence (where the Krylov subspace is spanned by the Lanczos vectors $\mathbf{v}_0 \dots \mathbf{v}_i$), we solve the system

$$\mathbf{C}\mathbf{w}_i = \mathbf{v}_i. \quad (4)$$

Since we seek a preconditioning operator with the property that $\mathbf{C}^{-1}\mathbf{A}$ approximates the identity matrix, we note that the preconditioning step, equation (4), is equivalent to obtaining an approximate solution to equation (2) when the source vector \mathbf{b} is replaced by the vector \mathbf{v}_i .

One approach to such an approximate solution is the “operator splitting” strategy (Trefethen and Bau 1996) for preconditioning. Briefly stated, if an operator \mathbf{A} can be decomposed in terms of the sum $\mathbf{A}_1 + \mathbf{A}_2 + \dots$, then sometimes a component \mathbf{A}_i or some subset of components can be used as an effective preconditioner. With respect to the EM induction problem at hand, we can impose a Helmholtz decomposition on the electric field ($\mathbf{E} = \mathbf{F} + \nabla f$) and precondition with a vector Laplacian operator \mathbf{L} (because $\nabla \cdot \mathbf{F} \equiv 0$) plus a divergence correction term \mathbf{q}_i (Smith, 1996):

$$\mathbf{C}^{-1}\mathbf{v}_i = \mathbf{L}^{-1}\mathbf{v}_i + \mathbf{q}_i. \quad (5)$$

This is precisely the LIN preconditioner (see Appendix), first described in Newman and Alumbaugh (2002), whereby the discrete Laplacian operator is symmetric and generated by centered finite differences. However, when generalized anisotropic media are present, as is the case here, the construction of the divergence correction term \mathbf{q}_i warrants further investigation since this involves a discretization \mathbf{P} of the $\nabla \cdot \bar{\sigma} \nabla$ operator—a task complicated by the presence of the anisotropic conductivity tensor $\bar{\sigma}$. A derivation of the LIN preconditioner (and thus the role of the $\nabla \cdot \bar{\sigma} \nabla$ operator) is contained in the Appendix.

Regarding the construction of a FD operator \mathbf{P} , we observe that for a given scalar potential f , the following relation holds in the continuous case:

$$\nabla \cdot \bar{\sigma} \nabla f = \sum_{\alpha, \beta}^{x, y, z} \frac{\partial}{\partial \alpha} \left[\sigma_{\alpha\beta} \frac{\partial f}{\partial \beta} \right], \quad (6)$$

where $\sigma_{\alpha\beta}$ are the individual terms in the symmetric 3×3 conductivity tensor $\bar{\sigma}$. An FD approximation to the individual terms of this summation follows from Weiss and Newman (2002) whereby an expectation value $\langle \cdot \rangle$ is defined over some region Ω :

$$\left\langle \frac{\partial}{\partial \alpha} \left[\sigma_{\alpha\beta} \frac{\partial f}{\partial \beta} \right] \right\rangle = \frac{1}{\Omega} \int_{\Omega} \frac{\partial}{\partial \alpha} \left[\sigma_{\alpha\beta} \frac{\partial f}{\partial \beta} \right] d\Omega. \quad (7)$$

Considering that the staggered FD grid defines electric field components along edges of the mesh and the fact that the LIN preconditioner relates the gradient of the scalar function f to the electric field, we define f at the nodes of the FD mesh (Figure 1). Thus, the region Ω is taken as $x_{i-1/2} < x < x_{i+1/2}$, $y_{j-1/2} < y < y_{j+1/2}$, and $z_{k-1/2} < z < z_{k+1/2}$. Evaluation of the integral for the case where $\alpha = \beta$ is relatively straightforward using centered differences. For example, the $\alpha = \beta = x$ term is given by

$$\left\langle \frac{\partial}{\partial x} \left[\sigma_{xx} \frac{\partial f}{\partial x} \right] \right\rangle = \frac{\Delta_{j-1/2}^y \Delta_{k-1/2}^z}{\Omega} \times \left[\frac{f_{i+1,j,k} - f_{i,j,k}}{\Delta_i^x} \sigma_{xx}(x_{i+1/2}, y_j, z_k) - \frac{f_{i,j,k} - f_{i-1,j,k}}{\Delta_{i-1}^x} \sigma_{xx}(x_{i-1/2}, y_j, z_k) \right], \quad (8)$$

where the node spacing Δ_{η}^{ξ} for coordinate ξ is given by $\xi_{\eta+1} - \xi_{\eta}$. The conductivity value σ_{xx} is taken to be a volume-weighted average of the σ_{xx} conductivities in the four FD cells surrounding the point $(x_{i+1/2}, y_j, z_k)$. For the remaining cases where $\alpha \neq \beta$, we take the volume element $d\Omega = d\alpha d\beta d\gamma$ and first write

$$\left\langle \frac{\partial}{\partial \alpha} \left[\sigma_{\alpha\beta} \frac{\partial f}{\partial \beta} \right] \right\rangle = \frac{1}{\Omega} \int_{\gamma_1}^{\gamma_2} \int_{\beta_1}^{\beta_2} \left[\sigma_{\alpha\beta} \frac{\partial f}{\partial \beta} \Big|_{\alpha_2} - \sigma_{\alpha\beta} \frac{\partial f}{\partial \beta} \Big|_{\alpha_1} \right] d\beta d\gamma. \quad (9)$$

Evaluation of the $\sigma_{\alpha\beta} \partial_{\beta} f$ terms follows next with the use of a four-point stencil, and the remaining integration over γ is approximated by scaling with the quantity $\Delta^{\gamma} = \gamma_2 - \gamma_1$. For

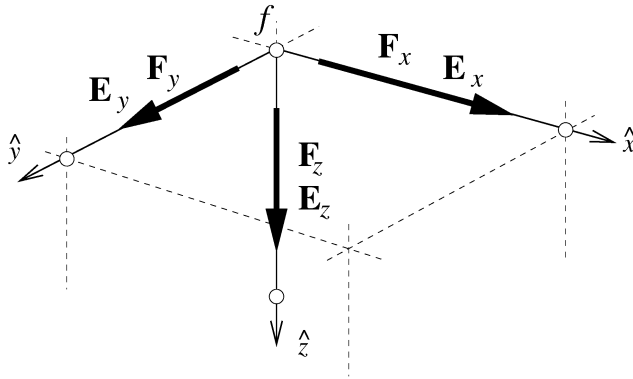


FIG. 1. Coordinate system used for FD discretization of equation (1) and the LIN preconditioner. Electric field components are sampled on the edges of the FD mesh whose nodes are represented by the open circles. Also sampled at the edges of the FD mesh are components FD solution of the vector Laplacian equation $\nabla^2 \mathbf{F} = -i\omega\mu\mathbf{J}$. In the calculation of the divergence correction term of the LIN preconditioner, values of the potential f are sampled at the FD nodes.

example, in the case where $\alpha = x$ and $\beta = y$, the right side of equation (9) becomes

$$\frac{\Delta_{k-1/2}^z}{\Omega} \left[\frac{f_{i,j+1,k} + f_{i+1,j+1,k} - f_{i,j,k} - f_{i+1,j,k}}{2/\sigma_{xy}(x_{i+1/2}, y_{j+1/2}, z_k)} + \frac{f_{i,j,k} + f_{i+1,j,k} - f_{i,j-1,k} - f_{i+1,j-1,k}}{2/\sigma_{xy}(x_{i+1/2}, y_{j-1/2}, z_k)} - \frac{f_{i-1,j+1,k} + f_{i,j+1,k} - f_{i-1,j,k} - f_{i,j,k}}{2/\sigma_{xy}(x_{i-1/2}, y_{j+1/2}, z_k)} - \frac{f_{i-1,j,k} + f_{i,j,k} - f_{i-1,j-1,k} - f_{i,j-1,k}}{2/\sigma_{xy}(x_{i-1/2}, y_{j-1/2}, z_k)} \right]. \quad (10)$$

Note that conductivity values in the expression above are required at the center of a FD cell face and are thus given by two-cell volume-weighted averages. Furthermore, when all the terms in equation (6) are evaluated in a similar fashion, the resulting 19-point stencil results in a symmetric FD coefficient matrix, provided that each of the individual equations in the system are scaled by the volume term Ω . This symmetrization step is analogous to those already documented in Newman and Alumbaugh (1995) and Weiss and Newman (2002).

Since the FD coefficient matrices \mathbf{L} and \mathbf{P} are real-valued and symmetric, solutions for \mathbf{F} and f are obtained by standard CG algorithms with an incomplete Cholesky factorization (ICF) used as preconditioner. Numerical instabilities in the factorization of \mathbf{P} for some problems motivate the use of a “shifted” Cholesky decomposition (Manteuffel, 1980) whereby the ICF of \mathbf{P} is replaced by the ICF of $\mathbf{P} + \chi \mathbf{I}$ and χ is taken heuristically as 0.001 times the maximum value on the diagonal of \mathbf{P} . Through numerical experimentation with the problems examined here, a stable ICF can arise with factors much greater than 0.001. However, it generally serves as poor preconditioner.

We close this section by noting that the divergence correction term in equation (5) renders the preconditioner \mathbf{C}^{-1} nonsymmetric. However, we note that since the divergence correction term is small, the preconditioner is “mostly” symmetric and, in practice, leads to a convergent QMR iterative sequence. For convenience, we can quantify the symmetry of the LIN preconditioner through a dimensionless symmetry quotient S_i ,

$$S_i = \frac{\|\mathbf{b}^T \mathbf{C}^{-1} \mathbf{A} \mathbf{x}_i\|}{\|(\mathbf{A} \mathbf{x}_i)^T \mathbf{C}^{-1} \mathbf{b}\|}, \quad (11)$$

where $\|\cdot\|$ denotes the L_2 norm. Clearly, in the case where \mathbf{C}^{-1} is symmetric, the quantity S_i is equal to unity. Furthermore, at minimal added computational cost, the effectiveness of the LIN preconditioner can be evaluated via a dimensionless quality factor Q_i ,

$$Q_i = \frac{\|\mathbf{C}^{-1} \mathbf{A} \mathbf{x}_i\|}{\|\mathbf{x}_i\|}, \quad (12)$$

which is equal to unity in the end member case where $\mathbf{C}^{-1} \mathbf{A}$ equals the identity matrix.

EXAMPLES

While the 3D FD solution to the anisotropy problem can accommodate a fully generalized anisotropy tensor (Weiss and Newman, 2002), a subclass of problems which is relevant to exploration geophysics is characterized by a conductivity tensor,

which, in the principal axes reference frame, consists of two components that are equal ($\sigma_{x'x'} = \sigma_{y'y'} = \sigma_{\parallel}$) and a third component ($\sigma_{z'z'} = \sigma_{\perp} < \sigma_{\parallel}$) whose value is smaller than the other two. This is the case in which σ_{\parallel} represents the conductivity in a plane (such as a sedimentary bedding plane), and the third, smaller component is the conductivity in the direction perpendicular to that plane. Orientation of the principal axes and, hence, the bedding plane with respect to the reference frame used for the model calculations is described by two Euler angles (Figure 2) corresponding to the “strike” and “dip” of the anisotropy. Thus, the previously developed 3D FD solution may find application in the modeling EM induction in, for example, a crossbedded sandstone unit.

The first example problem is shown in Figure 3a and consists of the double half-space model excited by a vertical magnetic dipole source embedded in the anisotropic region where the anisotropy dip angle θ is 60° [taken from Figure 6 in Anderson et al. (1998)]. Weiss and Newman (2002) report favorable agreement between the FD and analytic solutions to this

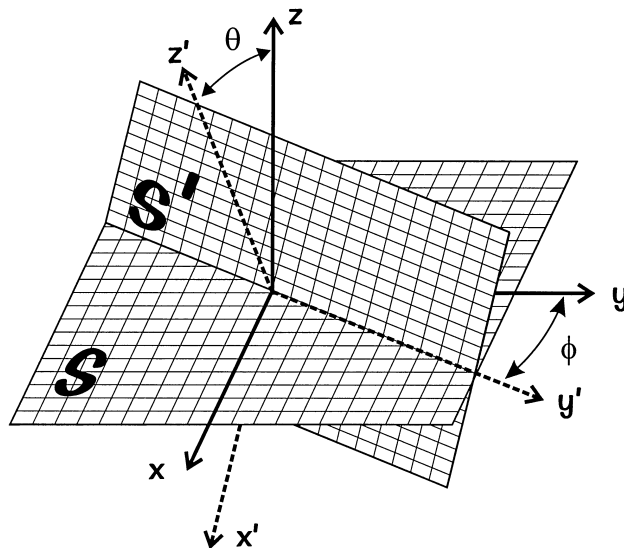


FIG. 2. Relationship between the x - y - z reference frame S and the x' - y' - z' principal axes reference frame S' where the electrical conductivity tensor is given by $\bar{\sigma}' = \text{diag}(\sigma_{\parallel}, \sigma_{\parallel}, \sigma_{\perp})$. Angles θ and ϕ represent the “dip” and “strike” of the x' - y' plane with respect to S .

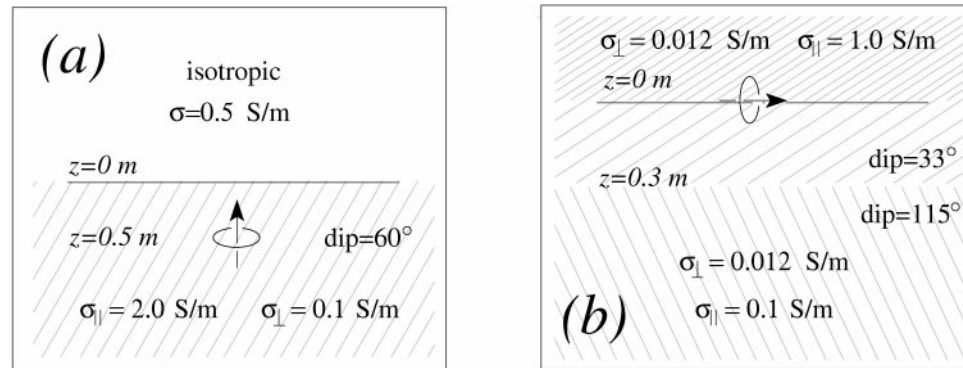


FIG. 3. Two models consisting of a single transmitter (symbol) embedded in an anisotropic medium (dip indicated by slanting lines). Transmitter frequencies for (a) and (b) are 20 kHz and 1 kHz, respectively. A comparison of FD results of model (a) with analytic solutions was previously reported in Weiss and Newman (2002).

model. For the present calculations, we discretized the region into $60 \times 60 \times 60$ FD cells over the region $-2 \text{ m} < x, y, z < 2 \text{ m}$ with a node spacing 0.1 m for $|x|, |y|, |z| > 1 \text{ m}$ and 0.05 m for $|x|, |y|, |z| < 1 \text{ m}$. Operating at an induction logging frequency of 20 kHz, the transmitter is embedded within the anisotropic region, 0.5 m below the half-space contact, and oriented such that its magnetic dipole moment is normal to the contact. Multiple solutions to this problem were generated by preconditioning with both a standard Jacobi preconditioner and the LIN preconditioner with varying tolerances of the accuracy of the ICF-CG solution. Plots of the quality factor Q_i , symmetry quotient S_i , and residual norm $\|\mathbf{b} - \mathbf{A}\mathbf{x}_i\|$ as a function of QMR iterate are shown in Figures 4 and 5. Computation times and QMR iterate counts are presented in Table 1.

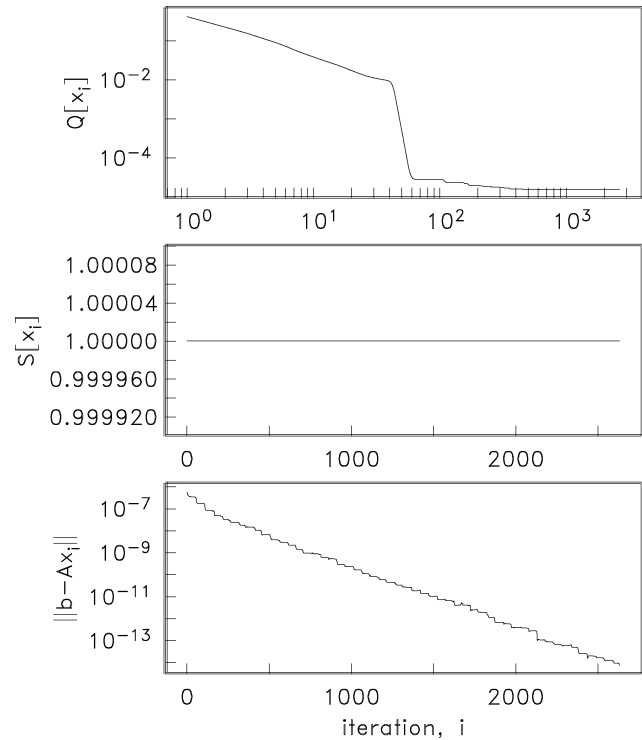


FIG. 4. Calculation of the quality factor (top), symmetry quotient (middle), and residual norm (bottom) for model (a) in Figure 3 using a Jacobi preconditioner.

The second example problem is shown in Figure 3b. It is composed of a 1-kHz horizontal magnetic dipole transmitter sandwiched between two layers with identical anisotropy dip, but different conductivity values in the principal axes reference frame. At a distance of 0.3 m below the transmitter and, hence, the interface between the two regions with different conductivity values, the orientation of the anisotropy dip changes from 33° to 115° , thus forming the bottommost

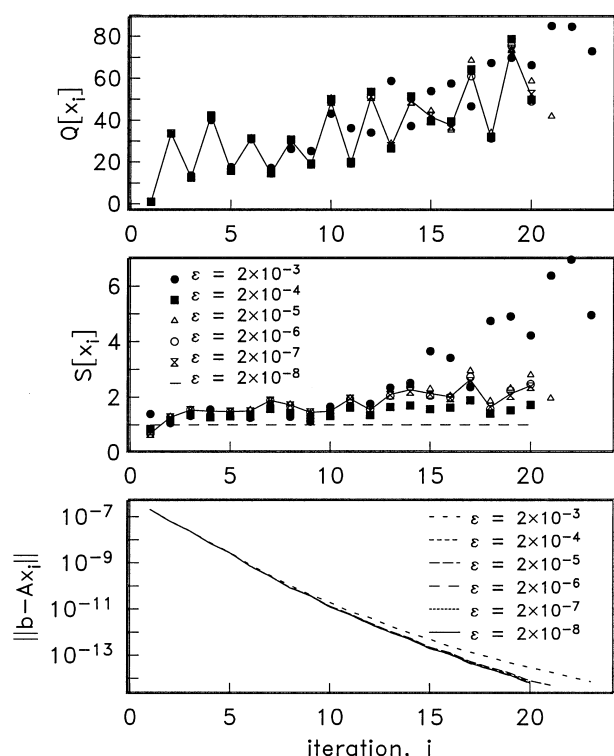


FIG. 5. Calculation of the quality factor (top), symmetry quotient (middle), and residual norm (bottom) for model (a) in Figure 3 using a LIN preconditioner. Results are shown for six different values of ICF-CG residual norm ε in the LIN preconditioner step. The dashed line in the middle figure is the ideal case of $S_i = 1$ for a perfectly symmetric preconditioner.

interface in this three layer model. The region is discretized a uniform $21 \times 21 \times 21$ mesh on $1 \text{ m} < x, y, z < 1 \text{ m}$. As with the previous model (Figure 3a), multiple solutions were computed using both the Jacobi preconditioner and LIN preconditioner with variable ICF-CG solution accuracy (Figures 6, 7; Table 1).

The final example problem we present (Figure 8) illustrates the variations in magnetic fields arising from a multicomponent induction log transmitter in a horizontal well. Electrical conductivity values σ_{\parallel} and σ_{\perp} are taken as spatially invariant. However, we introduce variations in the dip of the principal

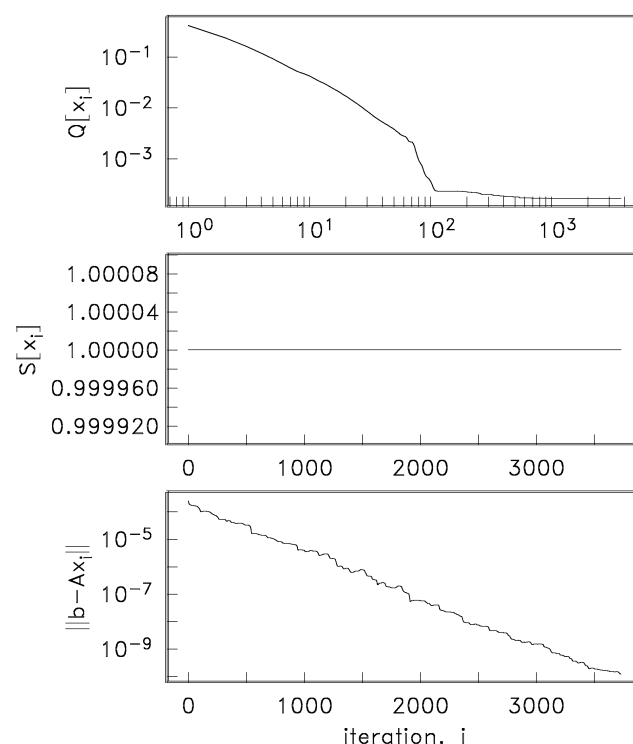


FIG. 6. Calculation of the quality factor (top), symmetry quotient (middle), and residual norm (bottom) for model (b) in Figure 3 using a Jacobi preconditioner.

Table 1. Summary of models evaluated and corresponding QMR performance attributes on a 1.5-GHz Athlon workstation. Number of nodes in the x , y , and z directions are denoted by N_x , N_y , and N_z , respectively. The number of degrees of freedom in the resulting FD system of linear equations is denoted by NDF . Solution accuracy in the LIN precondition steps is denoted by ε , which represents the final reduction in the residual by incomplete Cholesky factorization.

| Model | $N_x \times N_y \times N_z$ | NDF | C^{-1} | Time [s] | Iterates | $\ b - Ax_i\ /\ b\ $ |
|-------------|-----------------------------|--------|--------------------------------------|----------|----------|----------------------|
| Figure 3(a) | $61 \times 61 \times 61$ | 626580 | Jacobi | 2962 | 3726 | 4×10^{-7} |
| | | | LIN $\varepsilon = 2 \times 10^{-3}$ | 3099 | 111 | |
| | | | LIN $\varepsilon = 2 \times 10^{-4}$ | 607 | 19 | |
| | | | LIN $\varepsilon = 2 \times 10^{-5}$ | 685 | 19 | |
| | | | LIN $\varepsilon = 2 \times 10^{-6}$ | 810 | 20 | |
| | | | LIN $\varepsilon = 2 \times 10^{-7}$ | 949 | 21 | |
| | | | LIN $\varepsilon = 2 \times 10^{-8}$ | 1058 | 21 | |
| Figure 3(b) | $21 \times 21 \times 21$ | 21660 | Jacobi | 67 | 2631 | 1×10^{-8} |
| | | | LIN $\varepsilon = 10^{-3}$ | 14.5 | 23 | |
| | | | LIN $\varepsilon = 10^{-4}$ | 13.5 | 20 | |
| | | | LIN $\varepsilon = 10^{-5}$ | 15.3 | 21 | |
| | | | LIN $\varepsilon = 10^{-6}$ | 15.4 | 20 | |
| | | | LIN $\varepsilon = 10^{-7}$ | 16.5 | 20 | |
| | | | LIN $\varepsilon = 10^{-8}$ | 17.8 | 20 | |

axes reference frame to simulate the electrical structure of a crossbedded sandstone unit. The FD mesh is composed of 48×48 cells in the x - z plane and 41 cells in the y direction. Mesh spacing is a uniform 0.15 m in the y direction over $-3 \text{ m} < y < 3 \text{ m}$. Mesh spacing is also 0.15 m in the x and z directions for $|x|, |z| > 0.15 \text{ m}$, but is reduced to 0.01875 m for $|x|, |z| < 0.075 \text{ m}$ in order to better approximate a circular cross-section for a 0.15-m diameter borehole/invasion zone oriented along the y -axis. Along the y axis are a 20-kHz magnetic dipole transmitter at $y = -1 \text{ m}$ and a series of 21 receivers evenly distributed on $0 \text{ m} < y < 1 \text{ m}$. Magnetic field components from each of the x , y , and z polarizations of the transmitter are computed along with, for comparison, the fully coupled magnetic fields arising when the anisotropy dip variations in Figure 8 are set uniformly to 0° (Figure 9).

DISCUSSION

Clearly, the results in Table 1 demonstrate a significant reduction in the amount of CPU time required to solve the fully 3D EM induction problem when the LIN preconditioner is used instead of simple Jacobi scaling. Furthermore they illustrate that the solution of the vector Laplacian and scalar Poisson equations needn't be very accurate in order to generate an effective LIN preconditioner. Indeed, as these two systems are solved more accurately, the time required for construction of the LIN

preconditioner at each QMR iterate naturally increases but the number of QMR iterates remains essentially the same. Thus, effective use of the LIN preconditioner relies, in part, on choosing a ICF-CG solution tolerance that is sufficiently small, but not too small. In our experience, values on the order of 10^{-4} offer the best tradeoff for LIN accuracy versus time spent computing QMR iterates.

As noted earlier in the text, the divergence correction term \mathbf{q}_i [equation (5)] results in a LIN preconditioning operator that is nonsymmetric. However, the preconditioner is symmetric enough that the QMR iterative sequence still converges to a solution. While values of the symmetry quotient S_i for LIN preconditioning should be independent of the vectors \mathbf{Ax}_i and \mathbf{b} , uncertainty in the solution to the vector Laplacian equation (see Appendix) and the divergence correction term can lead to

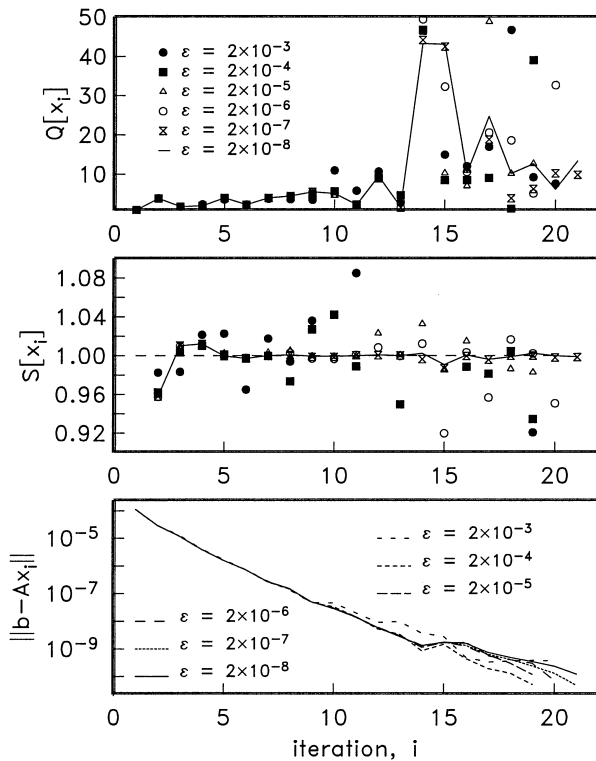


FIG. 7. Calculation of the quality factor (top), symmetry quotient (middle), and residual norm (bottom) for model (b) in Figure 3 using a LIN preconditioner. Results are shown for six different values of residual norm ϵ in the LIN preconditioner step (solution of both the vector Laplacian and Poisson equations).

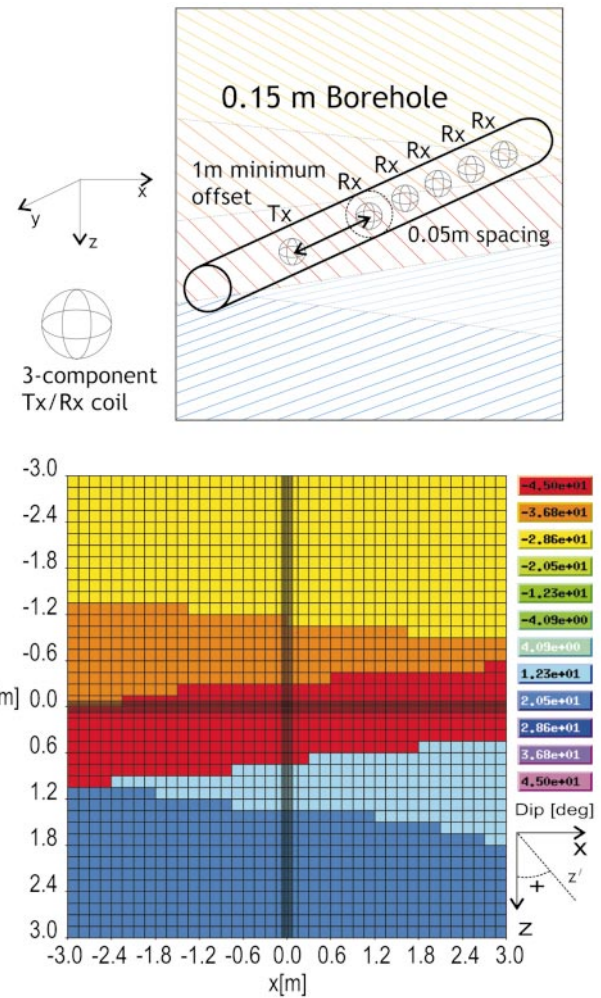


FIG. 8. (Top) Diagram (not to scale) of a y -directed horizontal well in a crossbedded sandstone whose EM response due to a multicomponent magnetic dipole transmitter (Tx) is computed at the receiver (Rx) locations along the borehole axis. (Bottom) Crosssection of the discretized crossbedded sandstone model with horizontal borehole. Shown here is the FD mesh in the x - z plane and the spatial variation in dip (here, y -invariant) of the principal axes reference frame. Formation conductivities are taken as $\sigma_{||} = 0.534 \text{ S/m}$ and $\sigma_{\perp} = 0.152 \text{ S/m}$ with a 0.15-m diameter y -directed borehole/invasion zone of $\sigma_h = \sigma_v = 0.285 \text{ S/m}$.

variations of S_i seen in Figures 5 and 7. It is worth noting, however, that they are generally close to unity for the two models presented and illustrate a minimum upper bound of $S_i \approx 6$ for QMR convergence. For comparison, variations in the Jacobi preconditioning (Figures 4 and 6) yields values $S_i = 1$ within machine tolerance. Admittedly, values of S_i which deviate from unity are difficult to interpret since theoretical bounds are not obvious from equation (11).

When compared to Jacobi scaling, the LIN preconditioner reduces the number of QMR iterates by more than two orders of magnitude for the models shown in Figure 3. This can be explained, in part, by examination of the quality factor Q_i (really, a lower-bound estimate of the \mathbf{x}_i -subordinate matrix 2-norm) for each of the preconditioning methods (Figures 4–7). In other words, Q_i is a measure of the magnification of the vectors \mathbf{x}_i by the operator $\mathbf{A}\mathbf{C}^{-1}$. Ideal values are of order one. Small values of Q_i indicate that the approximate solutions \mathbf{x}_i at each QMR iterate i reside very close to the null space of $\mathbf{C}^{-1}\mathbf{A}$, as appears to be the case with Jacobi preconditioning. This is in contrast to the case of LIN preconditioning where $\|\mathbf{C}^{-1}\mathbf{A}\| \geq 50$ for each of the two models examined.

One could interpret the convergence effect of the vectors \mathbf{q}_i within the context of inexact preconditioning (Golub and Ye, 1999). The idea of inexact preconditioning is such that the action of the preconditioner \mathbf{C}^{-1} is computed to some accuracy ϵ which, in general, is much less than the accuracy sought for the solution to the original set of linear equations. Thus, at each preconditioning step of the iterative sequence one would have $\mathbf{C}^{-1}\mathbf{v}_i + \mathbf{e}_i$, where \mathbf{e}_i is the error vector which can be

large ϵ is also large. This is similar in form, at least, to the expression given by equation (4). As an alternative to the two-term coupled recursion QMR algorithm used here (Freund and Nachtgal, 1994), a “flexible” QMR algorithm has been proposed by Szyld and Vogel (2001) which directly accounts for the vectors \mathbf{e}_i (or in our case, \mathbf{q}_i) at each iteration.

Lastly, an important application of the LIN preconditioner is shown by the results of Figure 9 for the multicomponent induction sonde in a horizontal well (Figure 8). Regarding solution of the linear system, one which was particularly ill-conditioned, the factor of 10^{-7} reduction in the residual norm (used in the previous examples) was unobtainable by Jacobi preconditioning after 5000 QMR iterations for each of the three transmitter polarizations. In contrast, the LIN preconditioner was able to generate a solution after approximately 20 iterations. The results (Figure 9) illustrate the fact that in an anisotropic medium where the conductivities in the “bed parallel” and “bed perpendicular” directions are spatially uniform, variations in the orientation of the bedding plane can generate nonzero secondary magnetic fields on the borehole axis in a null-coupled transmitter-receiver configuration. This, in itself, is nothing new and is presently in use by the induction logging industry to determine the relative orientation of bedding planes to the borehole axis (Beard et al., 1998; Gupta et al., 1999). However, these results demonstrate that a local 1D interpretation of the null-coupled response can be misleading, even in this relatively simple model where the fully 3D nature of the formation is clearly evident by the separation in the H_{yy} and H_{yy}^* curves in Figure 9b.

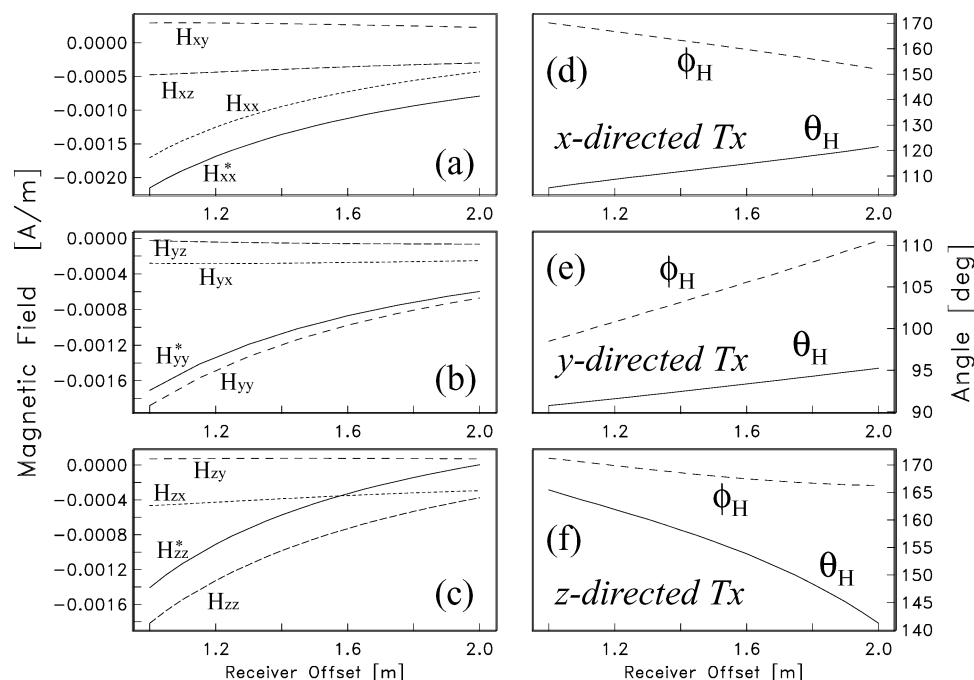


FIG. 9. (a)–(c) Plotted as a function of transmitter-receiver offset along the y -directed borehole axis shown in Figure 8, H_{ij} represents the j th quadrature component of magnetic field due to a unit-magnitude, multi-component 20-kHz transmitter with magnetic dipole moment oriented in the i th direction. Components labeled H_{ij}^* represent the fully coupled quadrature component of magnetic field when dip variations shown in Figure 8 are set uniformly to 0° . (d)–(f) Corresponding plots of the polar angle $\theta_H = \cos^{-1}(H_{iz}/|\mathbf{H}_i|)$ and azimuthal angle $\phi_H = \cos^{-1}(H_{ix}/|\mathbf{H}_i| \sin \theta_H)$ of magnetic field orientation along the borehole axis for an i -directed transmitter (Tx) moment in the presence of the crossbedded anisotropy shown in Figure 8.

CONCLUSIONS

A novel (LIN) preconditioner is presented for linear systems of equations arising from FD modeling of EM induction in a fully generalized 3D anisotropic medium. This work builds upon previous efforts in FD modeling of EM induction in an anisotropic medium (Weiss and Newman, 2002) and novel preconditioning strategies (Newman and Alumbaugh, 2002). Similar to the results found by Newman and Alumbaugh (2002) for transversely anisotropic media, we find that the LIN preconditioner can reduce the number of QMR iterations by two orders of magnitude and reduce the total QMR iterative sequence time by a factor of four when compared to Jacobi scaling. Furthermore, we note that the FD template developed here for the construction of the divergence correction term can be applied directly to the problem of dc resistivity sounding in a generalized 3D anisotropic medium. Also presented are results for a multicomponent EM induction sonde in a horizontal well, which were made possible through LIN preconditioning and underscore the challenges faced by the log analyst when confronted with an anisotropic formation. Combined, these results show that effective preconditioning can lead to previously unobtainable results and significantly reduce the solution times for 3D simulations, thus reducing the computational burden of 3D finite difference methods for electromagnetic imaging of geologic formations.

ACKNOWLEDGMENTS

The authors extend thanks to the Department of Energy's Natural Gas and Oil Technology Partnership and our industry collaborators for continued support of this project: Baker Hughes, Chevron, Electromagnetic Instruments Inc., Exxon-Mobil, Halliburton Energy Services, Pathfinder, and Schlumberger. This work was supported by the United States Department of Energy under Contract DE-AC04-94AL85000. Sandia is a multiprogram laboratory operated by Sandia Corporation, a Lockheed Martin Company, for the United States Department of Energy.

REFERENCES

- Anderson, B. I., Barber, T. D., and Gianzero, S. C., 1998, The effect of crossbedding anisotropy on induction tool response: 39th SPWLA Logging Symp., Expanded Abstract, Paper B.
- Beard, D. R., van der Horst, M., Strack, K.-M., and Taborovsky, L. A., 1998, Electrical logging of a laminated formation: International Patent WO 98/00733.
- Berg, R. R., 1986, Reservoir sandstones: Prentice Hall Inc.
- Christensen, N. B., 2000, Difficulties in determining electrical anisotropy in subsurface investigations: Geophys. Prosp., **48**, 1–19.
- Davydycheva, S., and Druskin, V., 1999, Staggered grid for Maxwell's equations in 3-D anisotropic media, in Oristaglio, M. and Spies, B., Eds., Three-dimensional electromagnetics: Soc. Expl. Geophys., 119–137.
- Druskin, V., and Knizhnerman, L., 1988, A spectral semi-discrete method for the numerical solution of 3-D non-stationary problems in electrical prospecting: Izv. Acad. Sci. USSR, Phys. Solid Earth, **8**, 63–74 (Russian; translated into English).
- Druskin, V. L., Knizhnerman, L. A., and Lee, P., 1999, New spectral Lanczos decomposition method for induction modeling in arbitrary 3-D geometry: Geophysics, **64**, 701–706.
- Everett, M. E., and Constable, S., 1999, Electric dipole fields over an anisotropic seafloor: Theory and application to the structure of 40 Ma Pacific Ocean lithosphere: Geophys. J. Internat., **136**, 41–56.
- Freund, R. W., and Nachtigal, N. M., 1994, An implementation of the QMR method based on coupled 2-term recurrences: SIAM J. Sci. Comput., **15**, 313–337.
- Glennie, K. W., 1972, Permian Rotliegendes of northwest Europe interpreted in light of modern desert sedimentation studies: AAPG Bull., **56**, 1048–1071.
- Golub, G. H., and Ye, Q., 1999, Inexact preconditioned conjugate gradient method with inner-outer iteration: SIAM J. Sci. Comput., **21**, 1305–1320.
- Gupta, P., Kriegshäuser, B., and Fanini, O., 1999, Conductivity anisotropy estimation method for inversion processing of measurements made by a transverse electromagnetic induction instrument: U. S. Patent 5999, 883.
- Klein, J. D., 1993, Induction log anisotropy corrections: Log Analyst, **34**, 18–27.
- LaBreque, D. J., 1999, Finite difference modeling of 3-D EM fields with scalar and vector potentials, in Oristaglio, M. and Spies, B., Eds., Three-dimensional electromagnetics: Soc. Expl. Geophys., 146–160.
- Mackie, R. L., Smith, J. T., and Madden, T. R., 1994, Three-dimensional electromagnetic modeling using finite difference equations: The magnetotelluric example: Radio Sci., **29**, 923–935.
- Manteuffel, T. A., 1980, An incomplete factorization technique for positive definite linear systems: Math. Comp., **34**, 473–497.
- Newman, G. A., and Alumbaugh, D. L., 1995, Frequency-domain modelling of airborne electromagnetic responses using staggered finite differences: Geophys. Prosp., **43**, 1021–1042.
- , 1996, Three-dimensional electromagnetic modeling on massively parallel computers: Sandia National Laboratories Report SAND96-0582.
- , 2002, Three-dimensional induction logging problems, Part 2: A finite-difference solution: Geophysics, **67**, 484–491.
- Smith, J. T., 1996, Conservative modeling of 3-D electromagnetic fields, Part II: Biconjugate gradient solution and an accelerator: Geophysics, **61**, 1319–1324.
- Steidmann, J. R., 1974, Evidence for eolian origin of cross stratification in sandstone of the Casper formation, southernmost Laramie Basin, Wyoming: AAPG Bull., **85**, 1835–1842.
- Szyld, D. B., and Vogel, J. A., 2001, FQMR: A flexible quasi-minimal residual method with inexact preconditioning: SIAM J. Sci. Comput., **23**, 363–380.
- Trefethen, L. N., and Bau, N., 1996, Numerical linear algebra: Soc. Ind. Appl. Math.
- Wang, T., and Fang, S., 2001, 3-D electromagnetic anisotropy modeling using finite differences: Geophysics, **66**, 1386–1398.
- Weidelt, P., 1999, Three-dimensional conductivity models: implications for electrical anisotropy, in Oristaglio, M. and Spies, B., Eds., Three-dimensional electromagnetics: Soc. Expl. Geophys., 119–137.
- Weiss, C. J., and Newman, G. A., 2002, Electromagnetic induction in a fully 3D anisotropic earth: Geophysics, **67**, 1104–1014.
- Yee, K. S., 1966, Numerical solution of initial boundary value problems involving Maxwell's equations in isotropic media: IEEE Trans. Ant. Prop., **14**, 302–307.
- Yu, L., Fanini, O. N., Kriegshäuser, B. F., Koelman, J. M. V., and van Popta, J., 2001, Enhanced evaluation of low-resistivity reservoirs using multi-component induction log data: Petrophys., **42**, 611–623.

APPENDIX

THE LIN PRECONDITIONER

Several authors have remarked on the difficulty in solving equation (1) as the frequency ω approaches the static limit (c.f., Druskin et al., 1999; LaBreque, 1999). One strategy for accommodating this difficulty begins with the Helmholtz theorem and the decomposition of electric field as the sum of divergence-free \mathbf{F} and curl-free ∇f parts:

$$\mathbf{E} = \mathbf{F} + \nabla f. \quad (\text{A-1})$$

Substituting equation (A-1) into equation (1) yields an equation in which the curl-curl operator of equation (1) is replaced by a vector Laplacian operator, as

$$-\nabla^2 \mathbf{F} + i\omega\mu\bar{\sigma}(\mathbf{F} + \nabla f) = -i\omega\mu\mathbf{J}. \quad (\text{A-2})$$

As pointed out in Newman and Alumbaugh (2002), the advantage of the Helmholtz decomposition is to deflate the null

space of the curl-curl operator, which is responsible for poor convergence rates when equation (2) is solved at low frequencies by iterative Krylov subspace methods. They note that the curl-curl operator is also responsible for the introduction of “spurious modes”, whereby the electric field \mathbf{E} can be augmented by the gradient of a scalar and still satisfy the discrete version of equation (1) [see Labreque (1999) for additional information on spurious modes].

Newman and Alumbaugh (2002) observed that when equation (A-2) is discretized on a FD grid of characteristic node spacing Δ , the elements of the discretized Laplacian operator are given approximately by $1/\Delta^2$. Thus, when the frequency ω is sufficiently small, the condition $1/\Delta^2 \gg \omega\mu\sigma$ is satisfied and a dimensionless “induction number” $\sqrt{\Delta^2\omega\mu\sigma}$ is much less than unity. Under these low induction number (LIN) conditions, the vector discrete Laplacian operator is likely to perform well as a preconditioner for the FD system of equations (2).

However, solution to the system $\nabla^2 \mathbf{F} = i\omega\mu\mathbf{J}$ yields a vector field which does not satisfy the continuity equation for electric currents. Thus, an equation for the scalar potential f in equation (A-1) can be derived from the application of the divergence operator to equation (2):

$$\nabla \cdot \bar{\sigma} \nabla f = -\nabla \cdot \bar{\sigma} \mathbf{F} - \nabla \cdot \mathbf{J}. \quad (\text{A-3})$$

Addition of the gradient of f to the vector field \mathbf{F} completes the construction of a low-frequency approximation to the fields described by equation (2). Derivation of a FD operator \mathbf{P} which approximates the continuous operator on the left side of the Poisson equation (A-3) is described in the main body of this paper. As noted earlier in equation (6), calculation of the divergence correction term is done by first solving equation (A-3) via finite differences, and then estimating the gradient of f by centered finite differences.